# Impact of nanostructuring on the magnetic and magnetocaloric properties of microscale phase-separated $La_{5/8-y}Pr_yCa_{3/8}MnO_3$ manganites

N. S. Bingham,[1] P. Lampen,[1] M. H. Phan,[1,*] T. D. Hoang,[2] H. D. Chinh,[2] C. L. Zhang,[3] S. W. Cheong,[3] and H. Srikanth[1,†]

[1]*Department of Physics, University of South Florida, Tampa, Florida 33620, USA*

[2]*Department of Inorganic Chemistry, Hanoi University of Science and Technology, Hanoi, Vietnam*

[3]*Rutgers Center for Emergent Materials and Department of Physics & Astronomy, Rutgers University, Piscataway, New Jersey 08854, USA*

(Received 30 March 2012; revised manuscript received 29 June 2012; published 16 August 2012)

Bulk manganites of the form $La_{5/8-y}Pr_yCa_{3/8}MnO_3$ (LPCMO) exhibit a complex phase diagram due to coexisting charge-ordered antiferromagnetic (CO/AFM), charge-disordered paramagnetic (PM), and ferromagnetic (FM) phases. Because phase separation in LPCMO occurs on the microscale, reducing particle size to below this characteristic length is expected to have a strong impact on the magnetic properties of the system. Through a comparative study of the magnetic and magnetocaloric properties of single-crystalline (bulk) and nanocrystalline LPCMO ($y = 3/8$) we show that the AFM, CO, and FM transitions seen in the single crystal can also be observed in the large particle sizes (400 and 150 nm), while only a single PM to FM transition is found for the small particles (55 nm). Magnetic and magnetocaloric measurements reveal that decreasing particle size affects the balance of competing phases in LPCMO and narrows the range of fields over which PM, FM, and CO phases coexist. The FM volume fraction increases with size reduction, until CO is suppressed below some critical size, ~100 nm. With size reduction, the saturation magnetization and field sensitivity first increase as long-range CO is inhibited, then decrease as surface effects become increasingly important. The trend that the FM phase is stabilized on the nanoscale is contrasted with the stabilization of the charge-disordered PM phase occurring on the microscale, demonstrating that in terms of the characteristic phase separation length, a few microns and several hundred nanometers represent very different regimes in LPCMO.

DOI: 10.1103/PhysRevB.86.064420 PACS number(s): 75.75.−c

## I. INTRODUCTION

Mixed phase manganites of the form $R_{1-x}M_xMnO_3$ ($R$ = La, Pr, Nd, Sm and $M$ = Sr, Ca, Ba, Pb) are strongly correlated systems in which competing interactions give rise to a variety of interesting phenomena,[1] including colossal magnetoresistance (CMR)[2] and a large magnetocaloric effect (MCE).[3] First gaining attention in the 1950's,[4] manganites continue to excite interest in the scientific community from the standpoint of both application and basic understanding.[5–7] The push for energy-efficient magnetic refrigeration based on a MCE has gained momentum in recent years, fueling further research into complex magnetic oxides.[3,6,7] Among the most intriguing properties exhibited by the manganites is the occurrence of spatial separation between regions of distinct magnetic ordering.[8–10] The sensitivity of such phase-separated systems to a variety of parameters including electric and magnetic field, strain, doping, and particle size introduces the potential for a large degree of tunability in magnetic and structural properties.[5,11,12]

Phase separation is most often observed between an insulating antiferromagnetic charge-ordered (CO) phase and a metallic ferromagnetic (FM) phase.[1] Charge ordering refers to the periodic arrangement of cations of different oxidation states within a crystal lattice, a common phenomenon in narrow bandwidth manganites in which long-range Coulomb interactions overcome the kinetic energy of the charge carriers.[13] While the electron-doped manganite compounds $La_{5/8}Ca_{3/8}MnO_3$ and $Pr_{5/8}Ca_{3/8}MnO_3$ exhibit FM and CO ground states, respectively, the combination of these two systems in $La_{5/8-y}Pr_yCa_{3/8}MnO_3$ (LPCMO) is known to generate a complex phase diagram involving microscale phase separation.[11,14–38] While phase separation between CO and FM regions in LPCMO has been well established, there is a growing body of evidence that an intermediate phase—charge-disordered paramagnetic (PM)—also influences the behavior of the system.[16,17,19,32,37] At temperatures below the onset of charge ordering, magnetic force microscopy (MFM) imaging suggests that $La_{0.25}Pr_{0.375}Ca_{0.375}MnO_3$ separates into PM and CO/PM regions.[23] Recently, the abrupt jump in magnetization below $T_C$ has been attributed to the sudden growth of FM domains within the charge-disordered PM phase rather than to the destabilization of CO regions to FM ordering.[37] Therefore the emerging picture incorporates three major coexisting phases in the region $T_C < T < T_{CO}$: FM, CO, and PM.

In LPCMO and related compounds, strain plays an integral role in the establishment of phase separation.[11,17,26–34] Previous investigations of mesoscopic properties in LPCMO suggest that reduced dimensionality can impact the strain landscape of the system.[17,18,27,34] Podzorov *et al.*[17] found that unaccommodated martensitic strain increased as the grain size in polycrystalline LPCMO was reduced from 17 to 3 $\mu$m, leading to the suppression of the metal-insulator transition (MIT) and the stabilization of the PM charge-disordered insulating (CD-I) phase. From a length scale comparable to the phase separation length, the observations of Singh-Bhalla *et al.*[34] crossed into the submicron regime in a study of magnetoresistance in patterned thin film bridges ranging from 5.0 to 0.6 $\mu$m in width. Below 2.5 $\mu$m, discrete steps began to emerge in the MIT and a downward shift in the transition temperature was evident below 0.9 $\mu$m. The widest range in sample dimension examined to date is found in a study by Deac *et al.*,[18] who prepared polycrystalline samples of LPCMO with different sintering temperatures, resulting in grain sizes between 200 nm and 4.2 $\mu$m that showed a

 

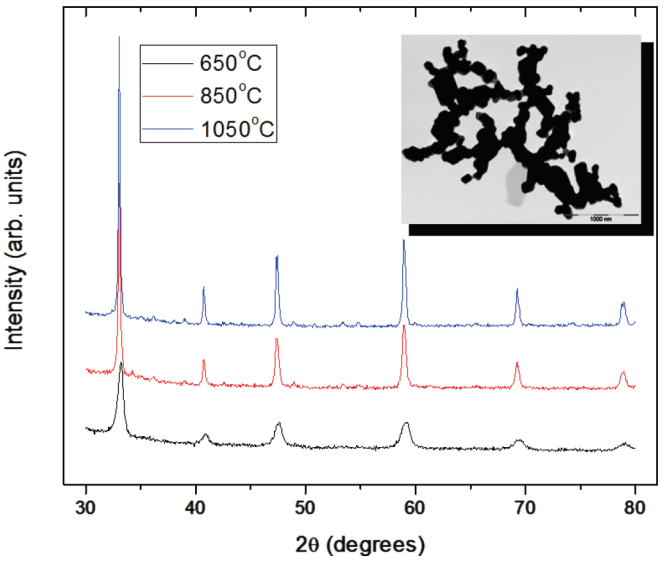


FIG. 1. (Color online) X-ray diffraction patterns of $La_{0.25}Pr_{0.375}Ca_{0.375}MnO_3$ nanoparticles annealed at 650, 850, and 1050 °C. A representative TEM micrograph of the particles annealed at 850 °C is shown in the inset.

continuous variation of phase fraction between FM and CO phases at low temperatures. We note that these studies of grain size reduction in polycrystalline LPCMO have not crossed the ∼100 nm threshold, below which surface effects dominate the physics of manganite nanoparticles.[39] With the exception of our previous study on a closely related composition,[40] we find that despite a wealth of available literature on thin films,[26–34,38] single-crystalline[16,19,22,23,25,37] and polycrystalline[11,14,15,17,18,20,21,41,42] forms of LPCMO, similar work done on nanoparticles of the same compounds is still lacking, although a reduction of particle size to well below the characteristic phase separation length can be expected to have a great impact on strain, and consequently on the magnetic properties of the system.[40]

TABLE I. Average particle size $\langle D \rangle$ and structural parameters for various annealing temperatures.

| $T$ (°C) | $\langle D \rangle$ (nm) | $a$ (Å) | $b$ (Å) | $c$ (Å) | $V$ (Å$^3$) | Mn-O-Mn (deg) |
|---|---|---|---|---|---|---|
| 650 | 55 | 5.4572 | 7.6495 | 5.4097 | 225.83 | 167.5 |
| 850 | 150 | 5.4291 | 7.6761 | 5.4157 | 225.70 | 178.0 |
| 1050 | 400 | 5.4269 | 7.6733 | 5.4159 | 225.53 | 178.1 |

Adding an additional layer of interest, opposing surface-driven trends are observed in nanosized FM and CO compounds.[39,43,44] For a material with an FM ground state, the general trend upon reducing particle size to the nanoscale is a decrease in magnetization.[44] Defects, nonstoichiometry, and broken bonds near the surface contribute to spin disorder,

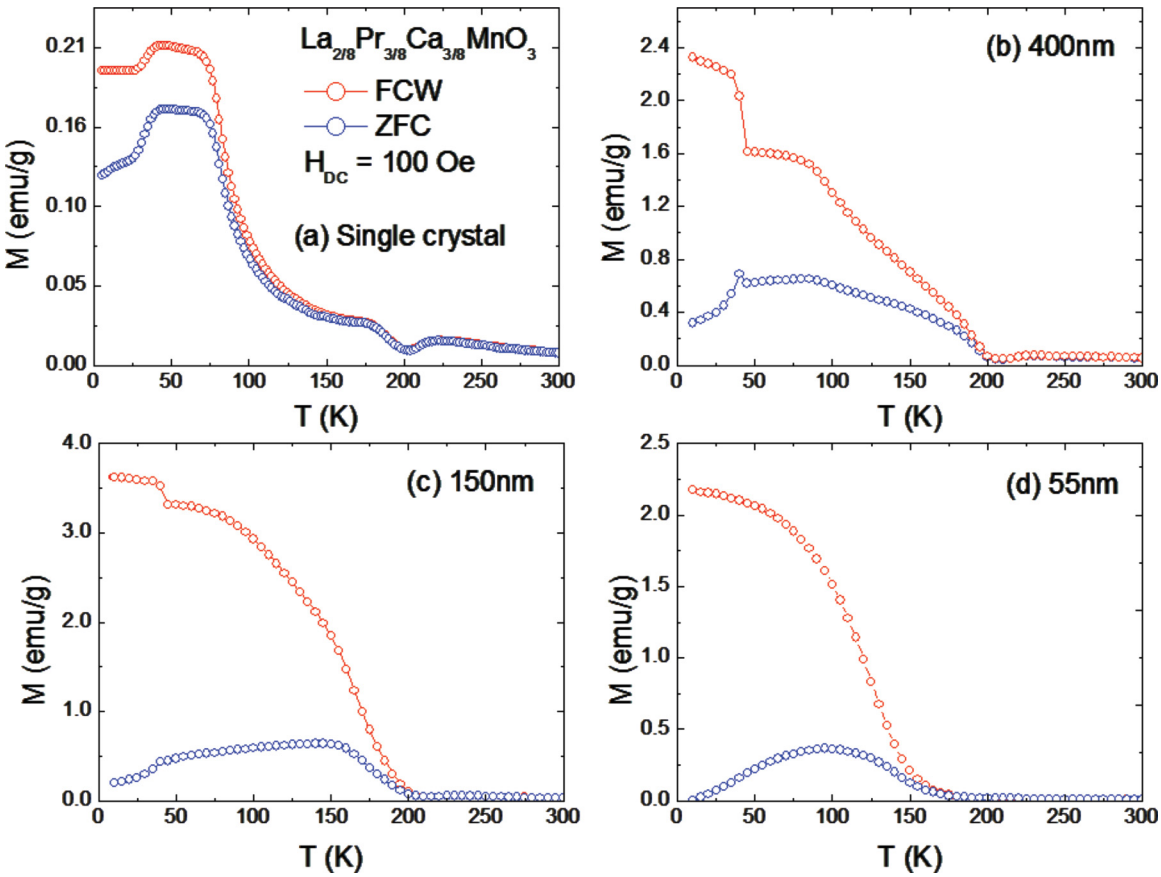


FIG. 2. (Color online) Field cooled (FC) and zero field cooled (ZFC) temperature-dependent magnetization curves for (a) single-crystal, (b) 400 nm, (c) 150 nm, and (d) 55 nm LPCMO in an applied dc field of 100 Oe.

i.e., a magnetically dead surface layer which becomes thicker with decreasing particle size. On the other hand, size reduction in materials with a CO ground state can result in enhanced magnetization as the AFM superexchange interaction associated with the CO phase is disrupted by uncompensated spins and inhomogeneous surface charge distribution, giving rise to an FM tendency at the surface of a CO nanoparticle.[39,45] This collapse of CO on the nanoscale is a particularly well-documented phenomenon in manganites, and has been observed in both materials with a single phase in the bulk form and those with two coexisting phases.[43,45–51] The presence of a third phase in LPCMO—the charge-disordered PM phase discussed above—lends a unique aspect to the study of nanoparticles of this compound as the impact of size reduction on the interplay of these three phases is not immediately obvious based on previous results.

In this study we examine the effects of systematically reducing particle size to the nanoscale in $La_{0.25}Pr_{0.375}Ca_{0.375}MnO_3$, a system whose bulk form comprises micron-sized regions of FM, PM, and CO phases. We find that the conflicting trends that accompany size reduction in nanoparticles of FM and CO manganites in combination with the mitigation of long-range phenomena (i.e., martensitic accommodation strains and microscale phase separation) result in a strong modification of the magnetic and magnetocaloric properties of LPCMO as particle size is decreased. The field sensitivity and balance of the coexisting phases is affected as the FM component is strengthened and becomes dominant below 100 nm. Our observation that the FM phase is stabilized on the nanoscale is contrasted with the earlier finding[17] that charge-disordered PM becomes dominant with grain size reduction on the microscale, demonstrating that in terms of the characteristic phase separation length, a few microns and several hundred nanometers represent very different regimes in microscale phase-separated LPCMO. A simple "geometric" model is proposed to illustrate the effects of particle size on the phase coexistence in LPCMO.

## II. EXPERIMENT

Nanocrystalline samples of $La_{0.25}Pr_{0.375}Ca_{0.375}MnO_3$ were prepared using a sol-gel method. Precursor solutions of lanthanum, praseodymium, calcium, and manganese nitrates were mixed in stoichiometric ratios. Citric acid was added to serve as a complexing agent of the metal ions, and the *p*H of the solution was controlled by the addition of $NH_3$. The solution was stirred at 80 °C, and then dried at 120 °C for a period of 24 h to obtain a gel. Calcination at 500 °C was performed to remove the organic materials. The resulting powder was then divided and annealed separately for 7 h

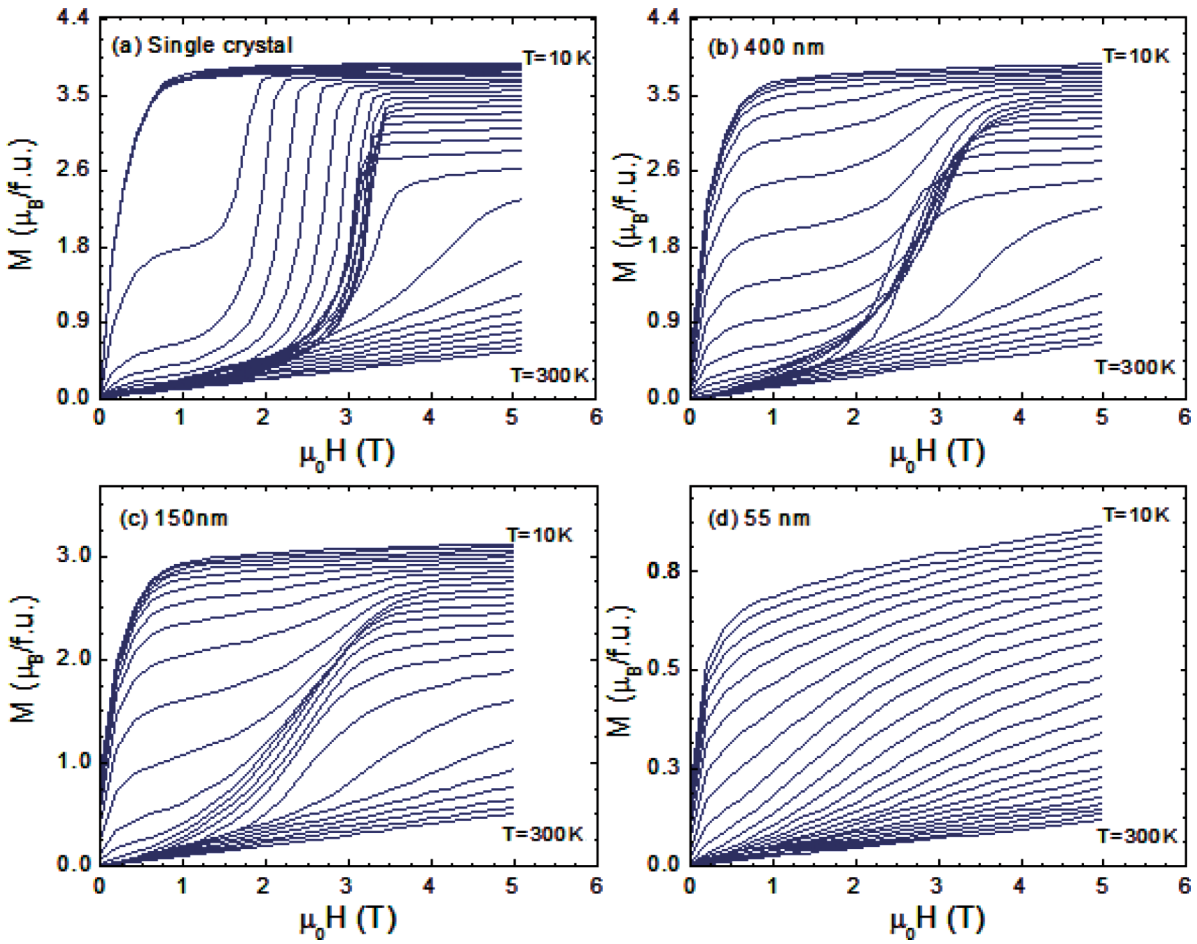


FIG. 3. (Color online) Magnetization vs field isotherms from 10 to 300 K and 0 to 5 T for (a) single-crystal, (b) 400 nm, (c) 150 nm, and (d) 55 nm LPCMO.

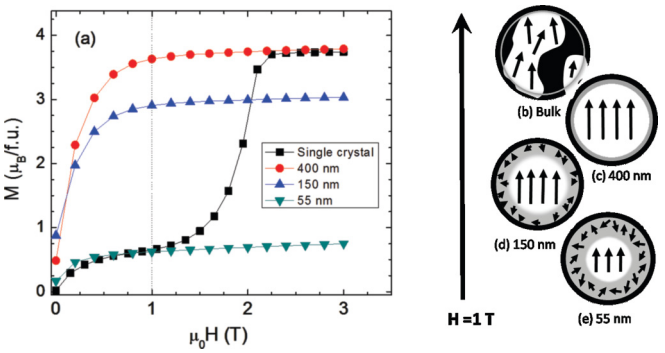


FIG. 4. (Color online) (a) Comparison of the field-dependent magnetization at 70 K up to 3 T. (b)–(e) represent the 1 T spin alignment within (b) the FM regions of the bulk sample and the FM particles in each nanocrystalline sample (c)–(e).

at 650, 850, and 1050 °C under the flow of oxygen gas to obtain nanoparticles of varying size. A single-crystal sample of $La_{0.25}Pr_{0.375}Ca_{0.375}MnO_3$ was prepared using an optical floating zone furnace. The phase purity of all samples was confirmed using x-ray diffraction (XRD). For the powders annealed at 650, 850, and 1050 °C, the average particle sizes were determined by XRD, scanning electron microscopy (SEM), and transmission electron microscopy (TEM) to be 55, 150, and 400 nm, respectively. Magnetic measurements were performed using a commercial Quantum Design Physical Properties Measurement System (PPMS) with a vibrating sample magnetometer over a temperature range of 5–300 K and fields up to 7 T. Magnetization isotherms were measured with a field step of 10 mT from 0 to 5 T, and a temperature step of 10 K in the range 10–300 K.

## III. RESULTS AND DISCUSSION

Figure 1 shows the XRD patterns of the nanocrystalline samples and a representative TEM image of the 150 nm sample. Structural refinements show that each sample belongs to the orthorhombic *Pnma* space group with lattice parameters reported in Table I. It can be seen that the unit cell volume expands slightly with reduction in particle size, a phenomenon that has been observed in other oxide systems,[52,53] and can be attributed to repulsion between unpaired surface electron orbitals. On the other hand, calculations[54] show that the Mn-O-Mn bond angle ($\theta$) decreases from the ideal 180° in the smallest particles, concurrent with a switch to the O′ subtype of the *Pnma* structure in which cooperative Jahn-Teller distortions occur in addition to the tilting of the $MnO_6$ octahedra.[55] As will be seen later, this structural shift occurs along with the suppression of the CO phase.

Figure 2 shows the zero field cooled (ZFC) and field cooled (FC) temperature-dependent magnetization of single-crystalline and nanocrystalline $La_{0.25}Pr_{0.375}Ca_{0.375}MnO_3$. The

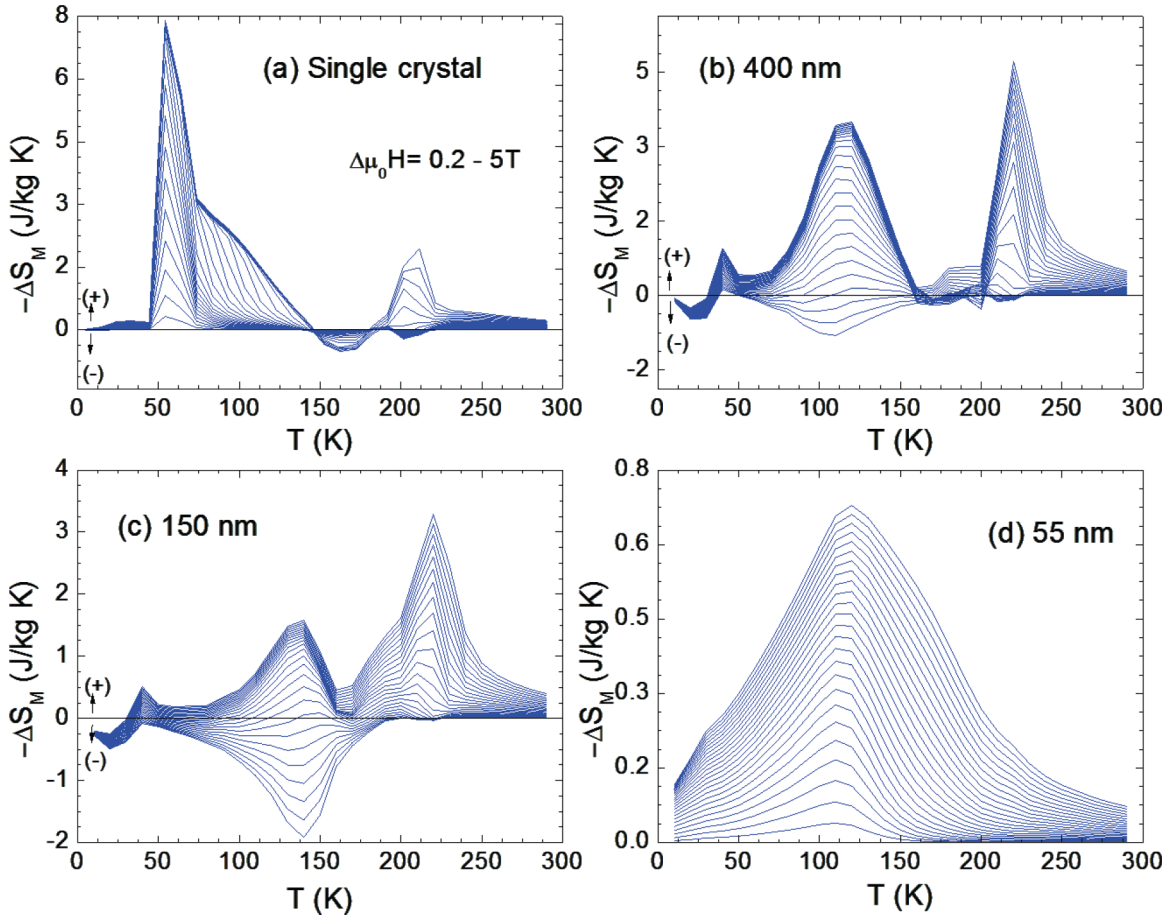


FIG. 5. (Color online) Temperature-dependent magnetic entropy change ($-\Delta S_M$) for fields between 0.2 and 5 T.

curves show several distinct transitions in the temperature range 10–300 K. In the single-crystal sample [Fig. 2(a)], the peak at ∼210 K and shoulder at ∼190 K correspond to charge-ordered paramagnetic (CO/PM) and charge-ordered antiferromagnetic (CO/AFM) transitions, respectively.[11,20] Long-range CO strains dominate the behavior of the crystal in the high temperature region, and the magnetization remains close to zero. However, near $T \sim 70$ K magnetization grows suddenly as competing interactions become close in energy, resulting in short-range order that is sensitive to thermal fluctuations. At low temperatures, the drop in magnetization at $T \sim 30$ K has been associated with a reentrant CO transition.[20]

The multitransitional nature of the system is preserved in the larger nanoparticle samples. From Figs. 2(b) and 2(c), it can be seen that many of the features observed in the single crystal persist in the 400 and 150 nm particles, but are strongly modified. Specifically, we note that there are two distinct phases to the growth of magnetization over the temperature interval: A gradual increase at intermediate temperatures is followed by a sharp jump at 50 K, similar to that observed in the single crystal. These features can be understood by considering that greater deviation from the average particle size was found in the samples annealed at higher temperatures ($\pm 150$, $\pm 50$, and $\pm 10$ nm for the 400, 150, and 55 nm samples, respectively). The largest particles ($>0.5$ $\mu$m) retain bulklike properties, including phase separation and a sharp transition to short-range order analogous to the magnetization jump in the single crystal. Thus the two phases of magnetization growth can be attributed to the extremes of the particle size distribution: In the smallest particles, the FM phase is stabilized and the particles align at high $T$, causing the gradual increase in magnetization while the sharp jump at lower $T$ is characteristic of the largest bulklike particles. The temperature at which the jump occurs shifts from ∼70 K in the single crystal to ∼50 K in the nanoparticles as the increased strain necessary to maintain phase separation in a small particle inhibits the sudden growth of the FM domains. As a general trend, we observe that the particles approach FM behavior as size is reduced. The relative size of the jump is reduced from 86% of total magnetization in the single crystal to 30% in the 400 nm particles and finally 8.5% in the 150 nm particles. From Fig. 2(d), only the signature of single-phase FM ordering is evident in the $M$-$T$ curves of the 55 nm particles. The trend of stabilization of the FM phase on the nanoscale contrasts with what occurs on the microscale (Podzorov *et al.*[17] showed that charge-disordered PM became dominant with grain size reduction on the microscale), demonstrating that in terms of the characteristic phase separation length, several hundred nanometers represents a very different regime from the microscale in LPCMO.

To examine these features in depth, isothermal magnetization curves were taken at temperatures between 10 and 300 K with a 10 K interval (Fig. 3). As suggested by the $M$-$T$ data, complex multiphase behavior is present in the single crystal, 400 nm, and 150 nm particles [Figs. 3(a)–3(c)], while the 55 nm particles [Fig. 3(d)] show only FM-like field dependence. The metamagnetic S-shaped isotherms in the larger sample sizes indicate the presence of multiple phases as the more field-sensitive FM and PM states become saturated at low fields, followed by the CO phase as field is increased. We note here that Deac *et al.*[18] estimated the FM phase fraction in LPCMO from the 5 K $M$-$H$ curves, and found an increase in

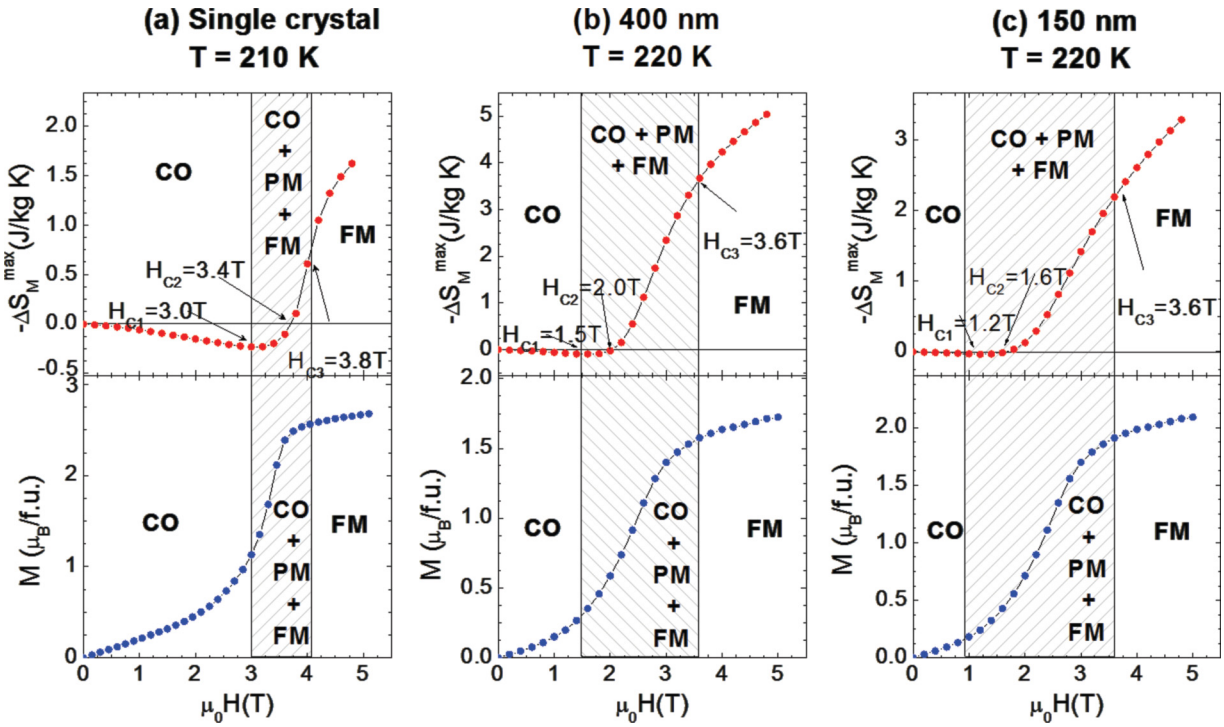


FIG. 6. (Color online) Magnetic field dependence of maximum magnetic entropy change ($-\Delta S_M^{\max}$) (a)–(c) and magnetization (d)–(f) near the charge ordering temperature. Phase coexistence occurs between $H_{C1}$, the field at which the CO phase begins to melt, and $H_{C3}$, the field at which the CO phase is fully converted to FM.

TABLE II. Comparison of field dependence of magnetic entropy change in bulk and nanocrystalline LPCMO.

| | $H_{C1}$(T) | $H_{C2}$(T) | $H_{C3}$(T) | Coexistence range ($H_{C3}$–$H_{C1}$)(T) | $-\Delta S_M^{max}(H_{C1})$ (J/kg K) | $-\Delta S_M^{max}$(5 T) (J/kg K) |
|---|---|---|---|---|---|---|
| Single crystal | 3.0 | 3.7 | 4.1 | 1.1 | −0.141 | 2.07 |
| 400 nm | 1.5 | 2.0 | 3.6 | 2.1 | −0.096 | 5.05 |
| 150 nm | 1.2 | 1.6 | 3.6 | 2.4 | −0.034 | 3.28 |

the FM phase with grain size. However, it is clear from Figs. 2 and 3 that an FM character dominates the low temperature regime of this material. Given that that larger grain size leads to enhanced magnetization in conventional FM materials, it is not surprising that 5 K data suggest an increased FM fraction in larger grains; applying the same method used in Ref. 16 to intermediate temperatures in the data of Fig. 3 would show an increase in the CO fraction.

In comparing the single crystal with the nanoparticles, it can be seen that the magnetization in the 400 nm particles reaches the same saturation value as in the single crystal ($\sim 3.8\mu_B$/f.u.); however, the nanocrystals show a greater sensitivity to small fields. This can be seen in the $M$-$T$ curves, and is consistent with Ref. 4, in which the smallest grain size showed a very large response to a small magnetic field. Figure 4(a) compares the $M$-$H$ curves of the single crystal and each particle size at 70 K. All nanocrystalline samples show increased field sensitivity over the bulk below 1 T, which can be attributed to the absence of long-range strains on the nanoscale and the enhancement of the FM component. With the reduction of particle size, surface spin disorder becomes increasingly significant [Figs. 4(b)–4(e)], reducing saturation magnetization in the 150 nm sample to $3.0\mu_B$/f.u. and preventing the 55 nm particles from reaching complete saturation in fields up to 5 T.

To further investigate the nature of the phase coexistence, magnetocaloric measurements were performed on each sample. In addition to characterizing a material's usefulness for refrigeration applications, MCE is a sensitive probe of magnetic phase transitions.[37,56] It is clear from the thermodynamic Maxwell relation,

$$\Delta S_M = \mu_0 \int_0^{H_{max}} \left(\frac{\partial M}{\partial T}\right)_H dH,$$

that entropy change is directly related to the first derivative of magnetization with temperature, making it inherently more sensitive to small changes in magnetization than $M$-$T$ or resistivity measurements alone. Upon integrating between the magnetization versus field curves, we observe distinct features in the temperature-dependent entropy change near the phase transition temperatures. By convention, we plot negative entropy change versus temperature. A PM to FM transition results in a positive peak in $-\Delta S_M$ as disordered spins align with an applied field and decrease the magnetic entropy. On the other hand, negative values of $-\Delta S_M$ are found for antiferromagnetic[37] and charge-ordered[57] transitions. Figure 5 shows the magnetic entropy change as a function of temperature for $\mu_0\Delta H = 0.2$–5 T in LPCMO. As expected, the $-\Delta S_M(T)$ curves show peaks around $T_{CO}$, $T_N$, and $T_C$ in all but the smallest particle size, in which a single PM to FM transition occurs. The presence of multiple peaks is a clear indication of the coexistence of CO and FM phases in the larger particles. The first two peaks, corresponding to $T_{CO}$ and $T_N$, show negative values for small applied fields. As $\mu_0\Delta H$ is increased, these peak values become large and positive, indicating that the balance of phases present in the sample is strongly field dependent.

To clarify the effect of applied field on the nature of the phase coexistence near the charge ordering transition, we plot the maximum magnetic entropy change ($-\Delta S_M^{max}$) as a function of field near $T_{CO}$ [Figs. 6(a)–6(c)]. The sign of $-\Delta S_M^{max}$ can be related to the relative quantities of the phases throughout the transition. In the small field range, $-\Delta S_M^{max}$ is negative and increases in magnitude up to a critical

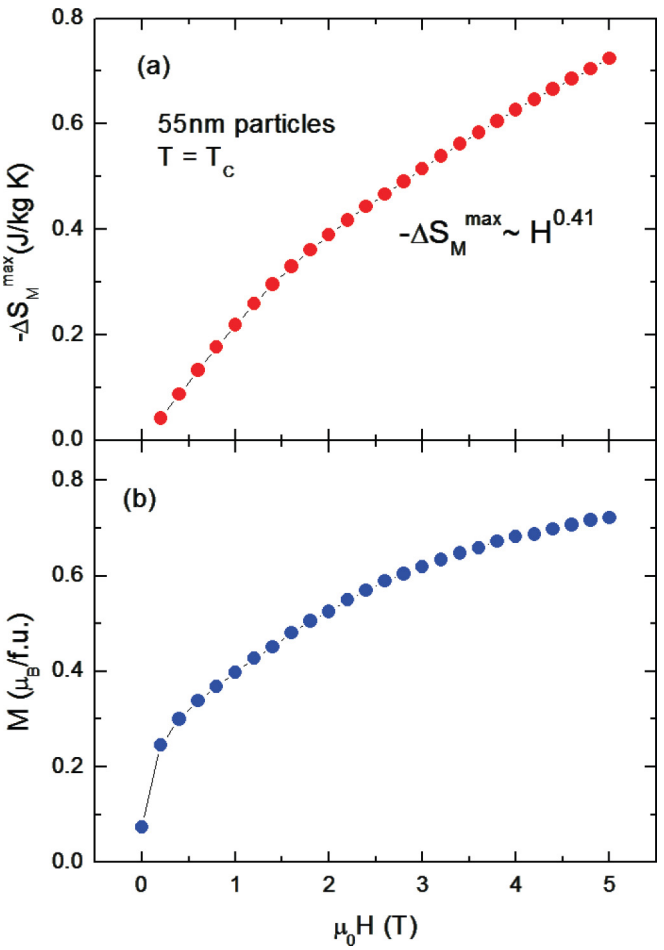


FIG. 7. (Color online) Magnetic field dependence of maximum magnetic entropy change ($-\Delta S_M^{max}$) (a) and magnetization (b) near $T_C$ for the 55 nm particles.

field ($H_{C1}$), then turns upward and crosses zero at a second critical field ($H_{C2}$). Below $H_{C1}$ the applied field is not strong enough to melt the CO phase, and its negative contribution to $-\Delta S_M^{\max}$ is dominant. In the region $H_{C1} < H < H_{C2}$, the positive contribution from the conversion of the PM phase into FM becomes significant so that at $H_{C2}$, the positive and negative effects of the three phases compensate one another and $-\Delta S_M^{\max}$ crosses zero. Above $H_{C2}$, $-\Delta S_M^{\max}$ increases rapidly with field as the CO phase is partially converted into the FM state. At $H_{C3}$, the full conversion of the CO to the FM state is accompanied by a change in slope. The critical values of $H_{C1}$, $H_{C2}$, and $H_{C3}$ correspond to those determined from the $M$-$H$ isotherm at the same temperature [Figs. 6(d)–6(f)].

Table II summarizes the results of Fig. 6. The range of fields over which the three phases coexist broadens from 1.1 T in the single crystal to 2.1 T in the 400 nm particles, and finally to 2.4 T in the 150 nm particles. It is also interesting to note that the onset of CO melting occurs at progressively lower fields as the sample size is reduced, shifting from 3.4 to 1.6 T. This is likely a consequence of increased field sensitivity that accompanies the absence of long-range strains on the nanoscale and the corresponding weakening of the CO phase. The maximum negative value that $-\Delta S_M^{\max}$ reaches also decreases in magnitude from 0.141 J/kg K in the single crystal to 0.034 J/kg K in the 150 nm particles. This trend agrees with our expectation that the volume fraction of CO becomes reduced in the nanocrystals and is therefore more readily balanced by the positive contributions from the other two phases.

In contrast to the critical behavior found in the single-crystal, 400 nm, and 150 nm samples, the maximum entropy change [Fig. 7(a)] and magnetization [Fig. 7(b)] in the 55 nm particles increase monotonically with field near $T_C$, as would be expected in a conventional ferromagnet. It can be seen that the high field data of Fig. 7(a) scale as $H^{0.41}$, which is a deviation from the $H^{0.67}$ dependence that mean field theory would predict for a long-range ferromagnetic material near a second order transition. It is possible that a small remnant of the CO phase persists even in the smallest particles, though not significant enough to be observed with the current techniques. However, the deviation from mean field behavior is more likely due to short-range magnetic ordering on the nanoscale combined with surface spin disorder.

Based on the observed magnetic and magnetocaloric behavior, the following scenario is proposed to explain the effects of particle size on the phase coexistence in $La_{0.25}Pr_{0.375}Ca_{0.375}MnO_3$ (see Fig. 8). Figures 8(a)–8(c) show the configuration of the phases in the single crystal at various temperatures. Below the Néel temperature, the sample is separated into microscale CO/AFM and PM regions [Fig. 8(a)]. As temperature is reduced further, FM domains nucleate and develop slowly within the PM phase [Fig. 8(b)], then grow rapidly at low $T$ [Fig. 8(c)], while the amount of the CO phase remains unaffected by temperature. Figures 8(d)–8(f) describe the corresponding behavior of the nanoparticles. In the largest particles, phase separation and bulklike behavior are retained. Among the smaller CO particles, an FM layer is established on the surface, thus reducing the volume fraction of the CO phase in favor of FM. In the absence of CO strains, the small PM particles convert easily to FM as temperature is decreased, generating the broad, gradual growth in magnetization seen in the $M$-$T$ curves. As size is reduced further [Figs. 8(g)–8(i)], few particles show phase separation and the CO volume fraction continues to decrease until below

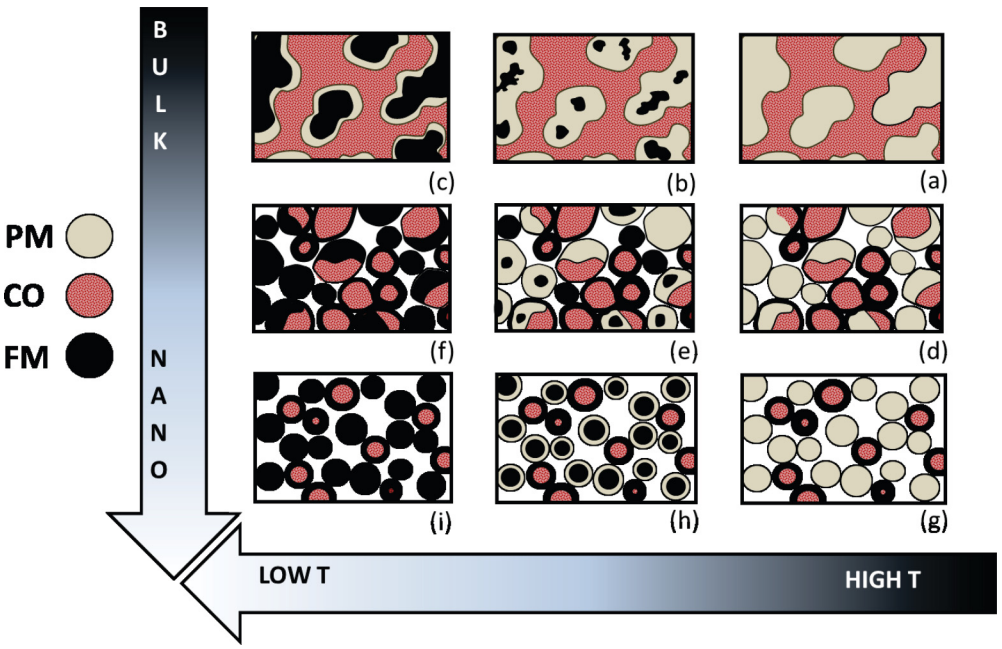


FIG. 8. (Color online) Size and temperature effects on phase coexistence in LPCMO. Paramagnetic (PM, cream), charge-ordered (CO, red), and ferromagnetic (FM, black) coexist in the temperature range $T_C < T < T_{CO}$. In the bulk, microscale phase separation occurs between PM and CO (a); FM domains nucleate in the PM phase and grow slowly (b) then suddenly (c) as $T$ is lowered. The FM volume fraction increases on the nanoscale (d)–(i) due to surface effects and weakening of the CO. Large particles exhibit bulklike behavior, while CO is suppressed in the smallest particles.

100 nm, contributions from the CO phase are insignificant, and only FM behavior is observed in $M$-$T$, $M$-$H$, and entropy change measurements.

## IV. CONCLUSIONS

We have studied the effects of size reduction in $La_{0.25}Pr_{0.375}Ca_{0.375}MnO_3$ by comparing the properties of the single-crystal sample with nanoparticles of average size 400 nm, 150 nm, and 55 nm. Magnetic and magnetocaloric experiments reveal phase coexistence in the bulk, 400 nm, and 150 nm particles while the 55 nm particles are single phase. The ferromagnetic volume fraction increases with size reduction, until charge ordering is suppressed below some critical size, ~100 nm. With size reduction, saturation magnetization and field sensitivity first increase as long-range charge ordering is inhibited, then decrease as surface effects become increasingly important. The trend that the FM phase is stabilized on the nanoscale is contrasted with previous observations of microscale behavior, demonstrating that in terms of the characteristic phase separation length, a few microns and several hundred nanometers represent very different regimes in LPCMO.

## ACKNOWLEDGMENTS

Work at USF was supported by DOE BES Physical Behavior of Materials Program through Grant No. DE-FG02-07ER46438. Work at Rutgers was supported by Grant No. NSF-BMR-1104484. Work at HUST was supported by NAFOSTED through Grant No. 104.02.74.09. M.H.P. also acknowledges the supports from the USF Internal Awards Program under Grant No. 68430 and the Florida Cluster for Advanced Smart Sensor Technologies (FCASST).

*phanm@usf.edu
†sharihar@usf.edu

[1] *Colossal Magnetoresistance, Charge Ordering and Related Properties of Manganese Oxides*, edited by C. N. R. Rao and B. Raveau (World Scientific, Singapore, 1998); *Colossal Magnetoresistance Oxides*, edited by Y. Tokura, Monographs in Condensed Matter Science (Gordon & Breach, New York, 1999).
[2] Y. Tokura and Y. Tomioka, J. Magn. Magn. Mater. **200**, 1 (1999).
[3] M. H. Phan and S. C. Yu, J. Magn. Magn. Mater. **308**, 325 (2007).
[4] J. B. Goodenough, Phys. Rev. **100**, 564 (1955).
[5] E. Dagotto, New J. Phys. **7**, 67 (2005).
[6] Z. B. Guo, Y. W. Du, J. S. Zhu, H. Huang, W. P. Ding, and D. Feng, Phys. Rev. Lett. **78**, 1142 (1997).
[7] P. Sarkar, P. Mandal, and P. Choudhury, Appl. Phys. Lett. **92**, 182506 (2008).
[8] J. Burgy, A. Moreo, and E. Dagotto, Phys. Rev. Lett. **92**, 097202 (2004).
[9] C. Sen, G. Alvarez, and E. Dagotto, Phys. Rev. Lett. **98**, 127202 (2007).
[10] V. B. Shenoy and C. N. R. Rao, Philos. Trans. R. Soc. London, A **366**, 63 (2008).
[11] M. Uehara, S. Mori, C. H. Chen, and S. W. Cheong, Nature (London) **399**, 560 (1999).
[12] K. H. Ahn, T. Lookman, and A. R. Bishop, Nature (London) **428**, 401 (2004).
[13] Y. Tomioka, A. Asamitsu, Y. Moritomo, H. Kuwahara, and Y. Tokura, Phys. Rev. Lett. **74**, 5108 (1995).
[14] M. Uehara and S.-W. Cheong, Europhys. Lett. **52**, 674 (2000).
[15] K. H. Kim, M. Uehara, C. Hess, P. A. Sharma, and S. W. Cheong, Phys. Rev. Lett. **84**, 2961 (2000).
[16] V. Kiryukhin, B. G. Kim, V. Podzorov, S.-W. Cheong, T. Y. Koo, J. P. Hill, I. Moon, and Y. H. Jeong, Phys. Rev. B **63**, 024420 (2000).
[17] V. Podzorov, B. G. Kim, V. Kiryukhin, M. E. Gershenson, and S. W. Cheong, Phys. Rev. B **64**, 140406 (2001).
[18] I. G. Deac, S. V. Diaz, B. G. Kim, S.-W. Cheong, and P. Schiffer, Phys. Rev. B **65**, 174426 (2002).
[19] H. J. Lee, K. H. Kim, M. W. Kim, T. W. Noh, B. G. Kim, T. Y. Koo, S.-W. Cheong, Y. J. Wang, and X. Wei, Phys. Rev. B **65**, 115118 (2002).
[20] P. A. Sharma, Sung Baek Kim, T. Y. Koo, S. Guha, and S. W. Cheong, Phys. Rev. B **71**, 224416 (2005).
[21] L. Ghivelder and F. Parisi, Phys. Rev. B **71**, 184425 (2005).
[22] C. Israel, W. D. Wu, and A. de Lozanne, Appl. Phys. Lett. **89**, 032508 (2006).
[23] W. Wu, C. Israel, N. Hur, S. Y. Park, S. W. Cheong, and A. Lozanne, Nat. Mater. **5**, 881 (2006).
[24] P. A. Sharma, S. El-Khatib, I. Mihut, J. B. Betts, A. Migliori, S. B. Kim, S. Guha, and S. W. Cheong, Phys. Rev. B **78**, 134205 (2008).
[25] M. Kim, H. Barath, S. L. Cooper, P. Abbamonte, E. Fradkin, M. Rübhausen, C. L. Zhang, and S. W. Cheong, Phys. Rev. B **77**, 134411 (2008).
[26] D. Gillaspie, J. X. Ma, H. Y. Zhai, T. Z. Ward, H. M. Christen, E. W. Plummer, and J. Shen, J. Appl. Phys. **99**, 08S901 (2006).
[27] T. Z. Ward, S. Liang, K. Fuchigami, L. F. Yin, E. Dagotto, E. W. Plummer, and J. Shen, Phys. Rev. Lett. **100**, 247204 (2008).
[28] T. Z. Ward, J. D. Budai, Z. Gai, J. Z. Tischler, Lifeng Yin, and J. Shen, Nat. Phys. **5**, 885 (2009).
[29] T. Dhakal, J. Tosado, and A. Biswas, Phys. Rev. B **75**, 092404 (2007).
[30] R. P. Rairigh, G. Singh-Bhalla, S. Tongay, T. Dhakal, A. Biswas, and A. F. Hebard, Nat. Phys. **3**, 551 (2007).
[31] S. H. Yun, T. Dhakal, D. Goswami, G. Singh, A. Herbard, and A. Biswas, J. Appl. Phys. **103**, 07E317 (2008).
[32] G. Singh-Bhalla, S. Selcuk, T. Dhakal, A. Biswas, and A. F. Hebard, Phys. Rev. Lett. **102**, 077205 (2009).
[33] J. Tosado, T. Dhakal, and A. Biswas, J. Phys.: Condens. Matter. **21**, 192203 (2009).
[34] G. Singh-Bhalla, A. Biswas, and A. F. Hebard, Phys. Rev. B **80**, 144410 (2009).
[35] H. T. Yi, T. Choi, and S. W. Cheong, Appl. Phys. Lett. **95**, 063509 (2009).
[36] J. Q. He, V. V. Volkov, T. Asaka, S. Chaudhuri, R. C. Budhani, and Y. Zhu, Phys. Rev. B **82**, 224404 (2010).
[37] M. H. Phan, M. B. Morales, N. S. Bingham, H. Srikanth, C. L. Zhang, and S. W. Cheong, Phys. Rev. B **81**, 094413 (2010).
[38] H. Jeen and A. Biswas, Phys. Rev. B **83**, 064408 (2011).
[39] T. Sarkar, B. Ghosh, A. K. Raychaudhuri, and T. Chatterji, Phys. Rev. B **77**, 235112 (2008).

[40]M. H. Phan, S. Chandra, N. S. Bingham, H. Srikanth, C. L. Zhang, S. W. Cheong, T. D. Hoang, and H. D. Chinh, Appl. Phys. Lett. **97**, 242506 (2010).
[41]A. L. L. Sharma, P. A. Sharma, S. K. McCall, S. B. Kim, and S. W. Cheong, Appl. Phys. Lett. **95**, 092506 (2009).
[42]M. Quintero, J. Sacanell, L. Ghivelder, A. M. Gomes, A. G. Leyva, and F. Parisi, Appl. Phys. Lett. **97**, 121916 (2010).
[43]C. L. Lu, S. Dong, K. F. Wang, F. Gao, P. L. Li, L. Y. Lv, and J. M. Liu, Appl. Phys. Lett. **91**, 032502 (2007).
[44]P. Kameli, H. Salamati, and A. Aezami, J. Appl. Phys. **100**, 053914 (2006).
[45]S. Dong, R. Yu, S. Yunoki, G. Alvarez, J. M. Liu, and E. Dagotto, Phys. Rev. B **78**, 201102 (2008).
[46]A. Biswas, T. Samanta, S. Banerjee, and I. Das, Appl. Phys. Lett. **92**, 012502 (2008).
[47]T. Sarkar, A. K. Raychaudhuri, and T. Chatterji, Appl. Phys. Lett. **92**, 123104 (2008).
[48]T. Zhang and M. Dressel, Phys. Rev. B **80**, 014435 (2009).
[49]S. Kundu, A. Das, T. K. Nath, and A. K. Nigam, J. Magn. Magn. Mater. **324**, 823 (2012).
[50]V. Markovich, I. Fita, A. Wisniewski, D. Mogilyansky, R. Puzniak, L. Titelman, C. Martin, and G. Gorodetsky, Phys. Rev. B **81**, 094428 (2010).
[51]V. Markovich, I. Fita, A. Wisniewski, D. Mogilyansky, R. Puzniak, L. Titelman, and G. Gorodetsky, J. Appl. Phys. **108**, 063918 (2010).
[52]P. Ayyub, V. R. Palkar, S. Chattopadhyay, and M. Multani, Phys. Rev. B **51**, 6135 (1995).
[53]S. Roy, I. Dubenko, D. D. Edorh, and N. Li, J. Appl. Phys. **96**, 1202 (2004).
[54]M. O'Keefe and R. G. Hyde, Acta Crystallogr. Sect. B **33**, 3802 (1977).
[55]J. A. Collado, C. Frontera, J. L. Garcia-Munoz, C. Ritter, M. Brunelli, and M. A. G. Aranda, Chem. Mater. **15**, 167 (2003).
[56]M. H. Phan, J. Gass, N. A. Frey, H. Srikanth, M. Angst, B. C. Sales, and D. Mandrus, Solid State Commun. **150**, 341 (2010).
[57]M. S. Reis, A. M. Gomes, J. P. Araujo, J. S. Amaral, P. B. Tavares, I. S. Oliveira, and V. S. Amaral, J. Magn. Magn. Mater. **290**, 697 (2005).